

# Impact of biexcitons on the relaxation mechanisms of polaritons in III-nitride based multiple quantum well microcavities

P. Corfdir,<sup>1,2,\*</sup> J. Levrat,<sup>1</sup> G. Rossbach,<sup>1</sup> R. Butté,<sup>1</sup> E. Feltin,<sup>1</sup> J.-F. Carlin,<sup>1</sup> G. Christmann,<sup>1,†</sup> P. Lefebvre,<sup>3,4</sup>  
J.-D. Ganière,<sup>1</sup> N. Grandjean,<sup>1</sup> and B. Deveaud-Plédran<sup>1</sup>

<sup>1</sup>*Institute of Condensed Matter Physics, Ecole Polytechnique Fédérale de Lausanne (EPFL), 1015 Lausanne, Switzerland*

<sup>2</sup>*Cavendish Laboratory, University of Cambridge, J. J. Thomson Avenue, Cambridge CB3 0HE, United Kingdom*

<sup>3</sup>*CNRS, Laboratoire Charles Coulomb, UMR5221, F-34095 Montpellier, France*

<sup>4</sup>*Université Montpellier 2, Laboratoire Charles Coulomb, UMR5221, F-34095 Montpellier, France*

(Received 8 February 2012; revised manuscript received 3 April 2012; published xxxxx)

We report on the direct observation of biexcitons in a III-nitride based multiple quantum well microcavity operating in the strong light-matter coupling regime by means of nonresonant continuous wave and time-resolved photoluminescence at low temperature. First, the biexciton dynamics is investigated for the bare active medium (multiple quantum wells alone) evidencing localization on potential fluctuations due to alloy disorder and thermalization between both localized and free excitonic and biexcitonic populations. Then, the role of biexcitons is considered for the full microcavity: in particular, we observe that for specific detunings the bottom of the lower polariton branch is directly fed by the radiative dissociation of either cavity biexcitons or excitons mediated by one LO-phonon. Accordingly, minimum polariton lasing thresholds are observed, when the bottom of the lower polariton branch corresponds in energy to the exciton or cavity biexciton first LO-phonon replica. This singular observation highlights the role of excitonic molecules in the polariton condensate formation process as being a more efficient relaxation channel when compared to the usually assumed acoustical phonon emission one.

DOI: 10.1103/PhysRevB.00.005300

PACS number(s): 78.67.De, 78.47.jd

## I. INTRODUCTION

In planar semiconductor microcavities (MCs), the strong coupling between excitons and photons gives rise to admixed quasiparticles called exciton polaritons.<sup>1</sup> Thanks to the unique properties coming from their dual light and matter nature, they raise great interest in the scientific community. We mention, for instance, parametric amplification,<sup>2</sup> massive occupation of the polariton ground state through Bose-Einstein condensation<sup>3</sup> or polariton lasing.<sup>4</sup> As a consequence, MC polaritons offer the possibility of achieving coherent light emission with a threshold lower than that of conventional semiconductor lasers<sup>5</sup> as it is not ruled by the Bernard-Duraffourg condition. The main limitation to achieve polariton lasing is the efficiency of the polariton relaxation from the excitonic reservoir to the bottom of the lower polariton (LP) branch (LPB).<sup>6</sup> To realize such a condensate under nonresonant excitation, the relaxation rate of polaritons from the exciton reservoir to the center of the Brillouin zone must indeed exceed their radiative decay.<sup>7,8</sup> However, due to their strong photonic character, LPs with a zero in-plane wave vector  $\mathbf{k}_{\parallel} = 0$  exhibit a radiative lifetime of the order of 0.1 to 10 ps, and it is therefore mandatory to inject a sufficiently high density of carriers to reach the stimulated scattering regime. In parallel, increasing the polariton density may lead to exciton screening and phase-space filling. Consequently, in GaAs MCs, the strong coupling regime (SCR) might be lost before reaching the nonlinear regime,<sup>9</sup> and great care must be taken when designing the MC sample so as to increase either the polariton lifetime,<sup>10</sup> the stability of polaritons,<sup>11</sup> or the interaction strength.<sup>12,13</sup>

On the contrary, the large exciton binding energy in GaN-based heterostructures shifts the Mott transition to much higher critical temperatures ( $T_{\text{crit}} \sim 540$  K)<sup>14</sup> and critical carrier densities [ $n_{\text{crit}} \sim 10^{12}$  cm<sup>-2</sup> per quantum well (QW),<sup>15</sup>] allowing

for the buildup of a polariton condensate at room temperature both in bulk<sup>4</sup> and multiple quantum well (MQW) nitride-based planar MCs.<sup>16</sup> It was shown experimentally<sup>17</sup> that the polariton lasing threshold critically depends on the temperature and the detuning  $\delta = E_c(0) - E_X(0)$ , with  $E_X(0)$  and  $E_c(0)$  the energy of the QW exciton and cavity photon at  $\mathbf{k}_{\parallel} = 0$ , respectively. Although such a behavior can be qualitatively described by accounting for the temperature- and  $\delta$ -dependences of the scattering rates by solving numerically semiclassical Boltzmann equations,<sup>14</sup> the system is definitely more complex. We mention, in particular, the role played by disorder,<sup>18,19</sup> dark exciton states, and biexcitons.<sup>20</sup> The latter have indeed been shown to be instrumental in analyzing four-wave mixing experiments performed on GaAs MCs.<sup>21–23</sup> The SCR between the biexciton transition and the cavity photon might even be observed in MCs submitted to intense circularly polarized excitation.<sup>24</sup> Compared to III-As or II-VI MQW MCs, disorder and biexcitons should play an even more important role in nitride-based systems. First, GaN MCs exhibit a significant disorder.<sup>25</sup> One, thus, expects a significant part of the oscillator strength from the LPs and the upper polaritons (UPs) to be shared with the uncoupled “dark” exciton modes in MQW MCs.<sup>26</sup> In addition, excitons confined in GaN QWs efficiently bind into biexcitons.<sup>27</sup> In bulk GaN, the biexciton binding energy is of the order of 5.7 meV.<sup>28,29</sup> In systems of reduced dimensionality, the biexciton binding energy varies in a non-trivial way as it depends on the confinement, the disorder, and the amplitude of the quantum-confined Stark effect inherent to III-nitride based heterostructures grown along the polar  $c$  axis.<sup>30</sup> In any case, in high-quality nitride-based MQW MCs, where the biexciton binding energy exceeds the exciton inhomogeneous broadening, it should be possible to observe additional emission features linked to the existence of biexcitons.<sup>20</sup> Alternatively, the formation of biexcitons could also play a

major role on the polariton laser threshold, as the LPB may be directly fed by the radiative dissociation of biexcitons.<sup>20</sup>

Here, we address the role played by biexcitons on the overall relaxation mechanisms in III-nitride MQW MCs by a combined reflectivity and photoluminescence (PL) study. We first observe biexciton emission from the bare-MQW active medium. In particular, we extract both biexciton binding and localization energies, and we describe the localization dynamics of biexcitons along the QW planes. We then turn our attention to the full-MC sample. Because of the disorder specific to III-nitride MC samples, polaritons partly share their oscillator strength with dark excitons, making it possible to observe these latter states via reflectivity and PL experiments. Next, we evidence that dark excitons efficiently bind into cavity biexcitons, which radiatively dissociate leaving an LP in the reservoir or a dark exciton. In the linear regime, when the energy of the first LO-phonon replica of the cavity biexciton matches that of the bottom of the LPB, an increase in the LP emission intensity at  $\mathbf{k}_{\parallel} = 0$  is observed. In addition, we observe for this detuning a minimum polariton lasing threshold. Consequently, in this specific detuning case, the relaxation of LPs toward the center of the Brillouin zone is limited by the radiative dissociation of cavity biexcitons rather than by the scattering of higher- $\mathbf{k}_{\parallel}$  LPs by acoustic phonons.

The paper is organized as follows. In Sec. II, we present the structure of the investigated samples and describe the experimental setups. In Sec. III, we identify the emission from biexcitons confined along the QW planes. We then describe how to obtain the biexciton binding and localization energies, an accurate determination of these two energies being mandatory to understand the role played by biexcitons in the full-MC sample. The emission properties of the MC sample are depicted in Sec. IV A, while the emission from cavity biexcitons is identified in Sec. IV B. The role played by biexcitons in the relaxation dynamics of LPs is discussed in Sec. IV C, and we draw our conclusions in Sec. V.

## II. EXPERIMENTAL DETAILS

We consider here separately a GaN-based MQW  $3\lambda$ -MC and its bare active medium, which consists of a 67-period GaN (1.2 nm)/Al<sub>0.2</sub>Ga<sub>0.8</sub>N (3.6 nm) stack. Both samples have been grown by metal organic vapor phase epitaxy (MOVPE)<sup>31</sup> on a 3  $\mu$ m thick GaN buffer deposited on a *c*-plane sapphire substrate. The first sample investigated here, i.e., the bare-MQW sample, was capped by a  $\lambda/4$  thick Al<sub>0.2</sub>Ga<sub>0.8</sub>N layer. The structure of the full MC, already described elsewhere (see Fig. 1 in Ref. 15 for a cross-section transmission electron micrograph of the sample), consists of a high-reflectivity epitaxial 35-pair lattice-matched Al<sub>0.85</sub>In<sub>0.15</sub>N/Al<sub>0.2</sub>Ga<sub>0.8</sub>N distributed Bragg reflector (DBR) grown on a strain relieving template made of two GaN/AlN superlattices separated by a GaN interlayer followed by an Al<sub>0.2</sub>Ga<sub>0.8</sub>N layer. We then grew on top of the bottom DBR the  $3\lambda$  active medium, consisting of the 67 QWs sandwiched between two  $\lambda/4$  Al<sub>0.2</sub>Ga<sub>0.8</sub>N layers. We finally deposited a 67 nm-thick Si<sub>3</sub>N<sub>4</sub> layer and a 13 pair top dielectric SiO<sub>2</sub>/Si<sub>3</sub>N<sub>4</sub> DBR. As previously shown in Refs. 15 and 16, the entire structure is crack-free. We emphasize that in this specific MC sample, polariton lasing has been reported over the whole 4 to 340 K temperature range for cavity

detunings comprised between 0 and  $-120$  meV under quasi-continuous-wave (cw) excitation as detailed in Refs. 14 and 17. Contrary to other MQW-based MC structures operating in the SCR, the present QWs are not located at the antinodes of the electromagnetic standing wave but homogeneously distributed over the full active region. This particular design has been chosen to remove from the QW emission any source of inhomogeneous broadening induced by the variation of the built-in electric field from one QW to the other.<sup>32</sup> We point out that both bare-MQW and full-MC samples have been grown during the same run. Consequently, it is likely that they exhibit similar barrier alloy disorder. We emphasize that the strain state of the GaN layers that constitute the QWs should, however, be different in the two samples, given the very different underlying layer morphology. More specifically, compared to the bare-MQW sample, the QWs in the MC sample are more compressively strained, and therefore their excitonic emission line will appear at higher energy (by  $\sim 60$  meV).

We notice that, although the present samples have been grown along the polar [0001] axis, we will hereafter neglect the effect of the built-in electric field on the relaxation and recombination mechanisms of excitons. Indeed these GaN QWs are thin enough to ensure an optimal overlap between electron and hole wave functions even in the presence of the electric field. To check this assumption, we have performed envelope function calculations in the effective potential formalism.<sup>33–35</sup> (Fig. 1). We have included a variational modeling of the exciton, in which we separate the in-plane and on-axis motions of the electron-hole pair.<sup>36</sup> We find that the dynamical descreening of the built-in electric field after pulsed photo-excitation<sup>37</sup> should affect neither the exciton binding energy ( $E_X^B = 43$  meV) nor the square modulus of the overlap integral between electron and hole wave functions ( $|\langle \Psi_e | \Psi_h \rangle|^2 = 0.9$ ), and therefore we expect no time- or excitation-dependent change of the exciton radiative lifetime.

Continuous-wave and quasi continuous-wave micro-PL studies were carried out using either a frequency-doubled Ar-ion laser ( $\lambda = 244$  nm) or a pulsed frequency-quadrupled Nd:YAG laser ( $\lambda = 266$  nm) with a repetition rate of 8.52 kHz and 500 ps pulse width. For the micro-PL experiments a UV microscope objective with a numerical aperture of 0.55 was used, and the laser beam was focused down to a spot diameter not larger than 2  $\mu$ m. The collected signal was sent to a 55 cm focal length monochromator followed by a liquid-nitrogen cooled UV-enhanced charge-coupled device. We estimate the spectral resolution of our system to be  $\sim 100$   $\mu$ eV. To image the eigenmode dispersion of the full MC, the back focal plane of the microscope objective (Fourier-plane) was imaged on the entrance slit of the spectrometer via two lenses with focal lengths of 30 and 20 cm, respectively. We also performed in the same configuration microreflectivity measurements with a 150 W Xe lamp (note that the experiments displayed in Fig. 5 have been taken with a two-arm goniometer in  $\theta$ - $\theta$  configuration, the incoming light beam being brought by a 100  $\mu$ m core fiber, while the reflected light was then collected by a 400  $\mu$ m core fiber; the overall setup offering an angular selection of  $1^\circ$ ). PL excitation (PLE) measurements were performed with an optical parametric oscillator- (OPO-) based laser system with an emission wavelength continuously tunable between 200 nm and 2.3  $\mu$ m pumped by a pulsed Nd:YAG laser

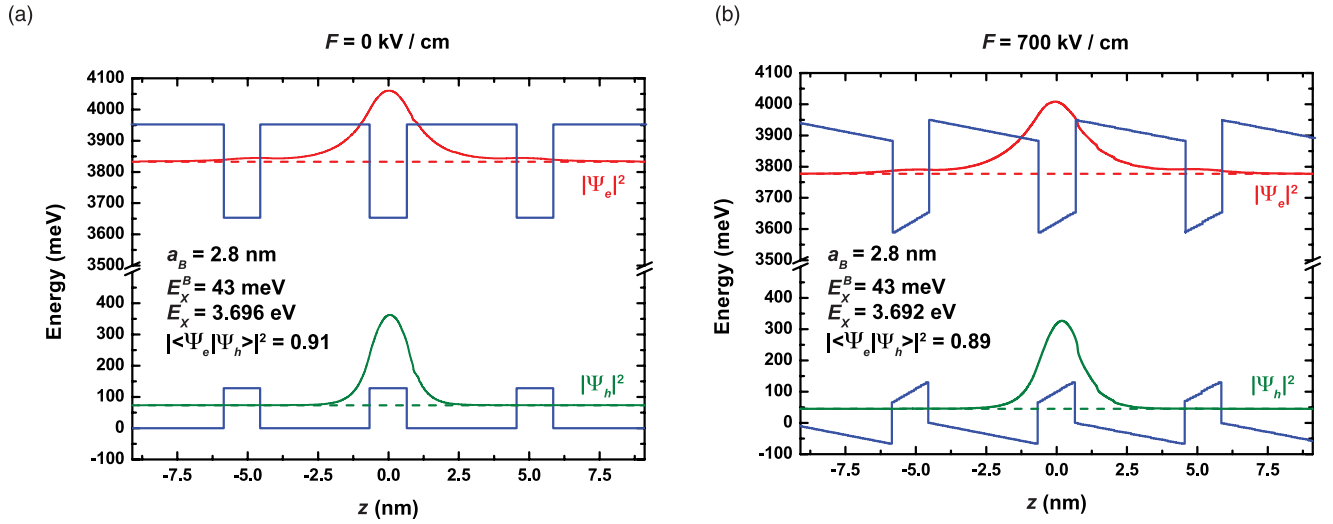


FIG. 1. (Color online) Band profiles (blue line) and electron and hole square modulus of the envelope functions [red (dark gray) and green (medium gray) curves, respectively] for an exciton confined in GaN (1.2 nm)/Al<sub>0.2</sub>Ga<sub>0.8</sub>N (3.6 nm) MQW without (a) and with built-in electric field (b). Dotted lines show the confined energy levels. We considered in (b) a 700 kV/cm built-in electric field, which is comparable to what has been observed in similar structures (Ref. 48).  $a_B$ ,  $E_X$ , and  $E_X^B$  are the exciton in-plane Bohr radius, transition energy, and binding energy, respectively, while  $|\langle \Psi_e | \Psi_h \rangle|^2$  is the square modulus of the overlap integral between electron and hole wave functions.

208 ( $\lambda = 355$  nm with a 1 kHz repetition rate and 3 ns pulse width).  
 209 Continuous-wave PL, reflectivity, and PLE experiments were  
 210 all carried out using a continuous-flow liquid-helium cryostat,  
 211 which allowed tuning the temperature from 4 to 300 K.  
 212 For all these experiments (PL, reflectivity, and PLE), we  
 213 estimate the spot diameter to be of the order of 4 to 5  $\mu$ m.  
 214 Time-integrated (TI) and time-resolved (TR) PL experiments  
 215 were carried out with the third harmonic of a Ti:Al<sub>2</sub>O<sub>3</sub>  
 216 mode-locked laser (pulse width and repetition rate of 2 ps and  
 217 80.7 MHz, respectively). For all TI and TR PL experiments,  
 218 the energy per excitation pulse was kept below 2 pJ. We tuned  
 219 the excitation wavelength to 280 nm in order to fall into a  
 220 reflectivity minimum of the Bragg reflector. The laser beam  
 221 was focused down to a 50  $\mu$ m-diameter spot on the sample  
 222 surface. The PL was analyzed with a 1200 grooves/mm  
 223 grating (spectral resolution of  $\sim 500$   $\mu$ eV) followed by an  
 224 Optronis streak camera working in synchroscan mode.

### 225 III. OPTICAL CHARACTERIZATION OF THE 226 MQW SAMPLE

227 In this section, we identify the emission from biexcitons  
 228 confined along the QW planes. We then extract both the  
 229 biexciton binding and localization energies from PL, PLE,  
 230 and reflectivity experiments and finally characterize by TR PL  
 231 the impact of interface roughness on the biexciton localization  
 232 dynamics. The observation of biexciton emission from the  
 233 MQW sample is demonstrated in Fig. 2. At 4 K, two  
 234 transitions lying at 3.655 and 3.639 eV dominate the spectrum  
 235 [Fig. 2(a)]. Under cw conditions, increasing the excitation  
 236 density leads to a superlinear increase in the intensity of  
 237 the lower-energy transition with respect to the emission at  
 238 3.655 eV [Fig. 2(a)]. Similarly to what was reported in Refs. 30  
 239 and 38, the power dependence of the emissions at 3.655 and  
 240 3.639 eV allows us to attribute them to the emission from the  
 241 fundamental QW exciton state (exciton A) and from biexcitons

(XX), respectively. Importantly, at low temperatures, the QW  
 242 emission properties are dominated by localized exciton ( $X_{loc}$ )  
 243 states,<sup>39</sup> and the exciton emission energy  $\Delta_X$  is given by:  
 244

$$\Delta_X = E_X - E_X^{loc}, \quad (1)$$

245 where  $E_X$  is the energy of free excitons (FXs) with an in-plane  
 246 wave vector  $\mathbf{k}_{\parallel} = 0$  and  $E_X^{loc}$  is the exciton localization  
 247 energy. In GaN QWs, potential fluctuations arise from single  
 248 or bilayer well width variations<sup>40</sup> as well as from barrier alloy  
 249 disorder.<sup>31</sup> While PLE and reflectivity measurements give  
 250 access to the energy of the (delocalized) excitonic resonances  
 251  $X_A$  and  $X_B$ , we observe by PL experiments the emission  
 252 from  $X_{loc}$  [Fig. 2(b)]. From the energy difference between  $X_A$   
 253 and  $X_{loc}$ , we deduce  $E_X^{loc} = 11$  meV [Fig. 2(b)]. This energy  
 254 seems quite small compared to the 40 meV that we calculate  
 255 by envelope function calculations for the localization energy  
 256 of an exciton on a single-monolayer well-width fluctuation.  
 257 As a matter of fact, it has already been shown that in  
 258 MOVPE-grown (Al,Ga)N/GaN QWs, Al-content fluctuations  
 259 in the (Al,Ga)N barriers play the most important role in the  
 260 QW emission inhomogeneous linewidth.<sup>31</sup> From the S-shaped  
 261 temperature-dependence of the (Al,Ga)N emission energy  
 262 [Fig. 2(c)], we extract an exciton localization energy of  
 263 30 meV in the disordered alloy.<sup>41</sup> We, therefore, account  
 264 for these fluctuations in the (Al,Ga)N energy band gap in  
 265 our calculations, and we find that they induce a QW exciton  
 266 localization energy of approximately 12 meV. In addition to  
 267 the emission from the (Al,Ga)N barriers and from X and XX  
 268 confined along the QW planes, we observe at 3.564, and 3.548  
 269 eV the emission from the X and XX first LO-phonon replica,  
 270 respectively, as well as the emission from the GaN buffer layer:  
 271 the donor-bound A-exciton centered at 3.481 eV and the FX  
 272 lines A and B at 3.488 and 3.497 eV, respectively [Fig. 2(b)].  
 273 Finally, although we observe by reflectivity and PLE a clear  
 274 resonance from the B QW exciton [Fig. 2(b)], we will hereafter  
 275 neglect its role on the relaxation and recombination processes

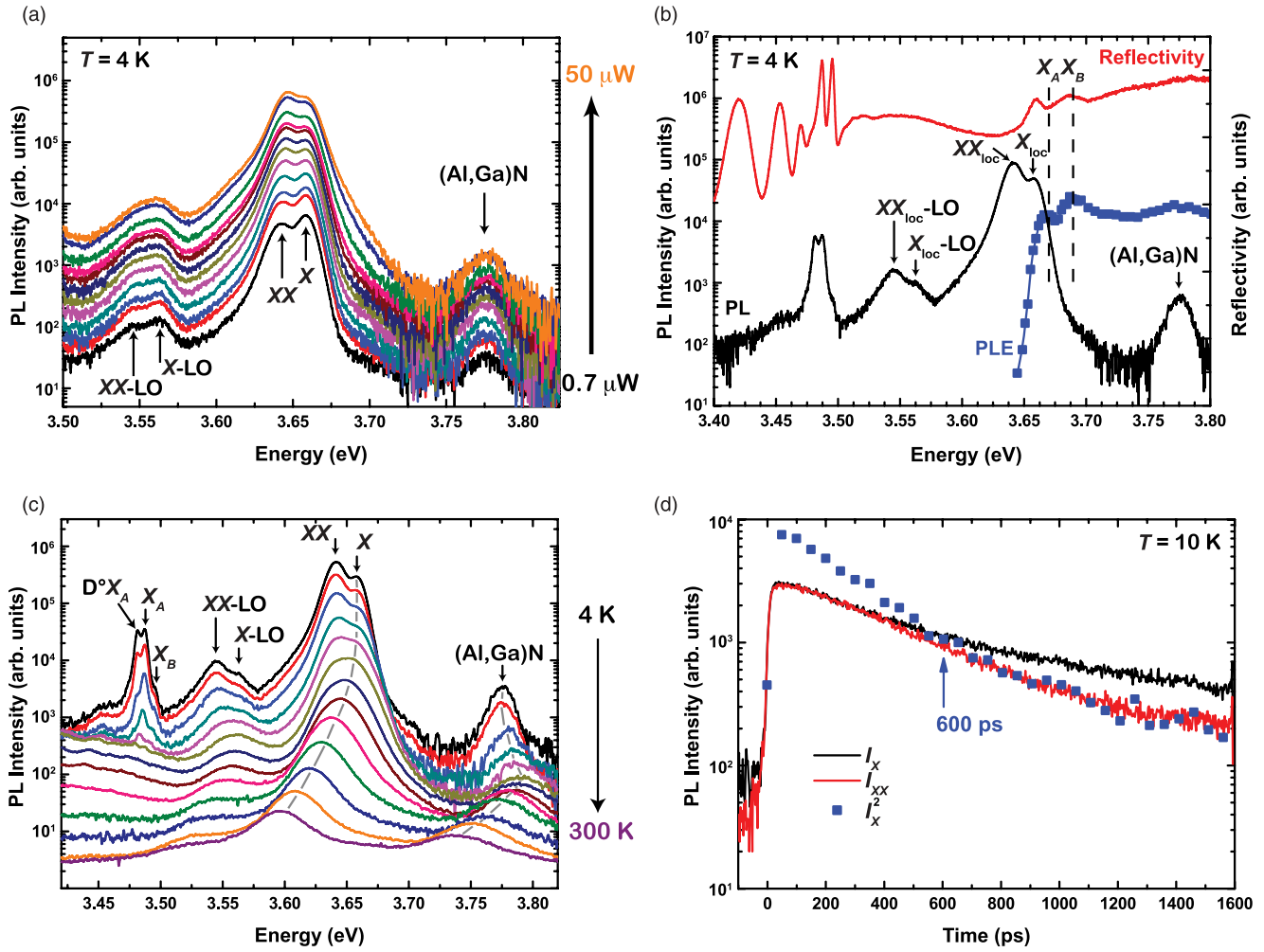


FIG. 2. (Color online) (a) Power-dependent PL spectra of the Al<sub>0.2</sub>Ga<sub>0.8</sub>N/GaN MQW sample measured at 4 K taken under quasi-cw conditions. The line at 3.639 eV shows a superlinear increase with excitation power with respect to that of the exciton (X), evidencing its biexcitonic origin. (b) Continuous-wave PL (black), reflectivity [red (dark gray)] and PLE [blue (medium gray)] spectra measured at 4 K. The energies of X<sub>A</sub> and X<sub>B</sub> are deduced from the deconvolution of the PLE spectrum. For the PLE spectrum, the wavelength of the excitation laser was scanned with a 0.2 nm step width. We deduce from the energy difference between PLE and PL spectra a localization energy of 11 meV for excitons confined in the MQWs. (c) Continuous-wave PL spectra for the Al<sub>0.2</sub>Ga<sub>0.8</sub>N/GaN MQWs from 4 to 300 K. Spectra have been shifted vertically for clarity. Increasing the temperature leads to a quenching of the biexciton emission. In (b) and (c), cw PL spectra have been taken with a frequency-doubled Ar<sup>+</sup> laser (λ = 244 nm) with an excitation power density of 175 W/cm<sup>2</sup>. Note also that in (b) and (c), the lines below 3.51 eV arise from the 3 μm thick GaN buffer. (d) Low-temperature PL time decays for the exciton (black) and biexciton [red (dark gray)] emissions. After 600 ps, the biexciton emission intensity follows the same time dependence as the square of the exciton emission intensity (blue symbols), evidencing full thermalization between exciton and biexciton states. Note that the biexciton PL decay has been spectrally integrated over the emission from free and localized biexcitons.

of carriers. We indeed measure an energy difference of 21 meV between A and B QW excitons. Therefore, for a lattice temperature of 10 K, this higher-energy exciton branch should not be thermally populated.

The biexcitonic origin of the 3.639 eV line is fully consistent with TR-PL data [Fig. 2(d)]. Indeed, at quasithermal equilibrium, exciton and biexciton emission intensities ( $I_X$  and  $I_{XX}$ , respectively) verify at all times  $I_X(t)^2 \propto I_{XX}(t)$  (see Appendix, where the validity of this expression is also shown between localized excitons and localized biexcitons). Experimentally, we observe that it takes ~600 ps for the mass action law between excitons and biexcitons to be satisfied. Such a long delay between biexciton formation and the realization of

thermal equilibrium between exciton and biexciton densities was previously attributed to the partial decoupling of exciton and biexciton dynamics, once these carriers are localized. Although the detailed discussion of the thermalization dynamics between excitons and biexcitons is outside the scope of this paper, we also presume that the thermalization time between excitons and biexcitons is related to the quantum-confined Stark effect and thus mainly depends on the thickness of the QW.

As it is the case for excitons, biexcitons are bound to potential fluctuations at low temperatures. We, thus, define the biexciton localization energy  $E_{XX}^{loc}$  as the energy difference between biexcitons free to move along the QW plane and biexcitons bound to potential fluctuations [Fig. 3(a)], giving

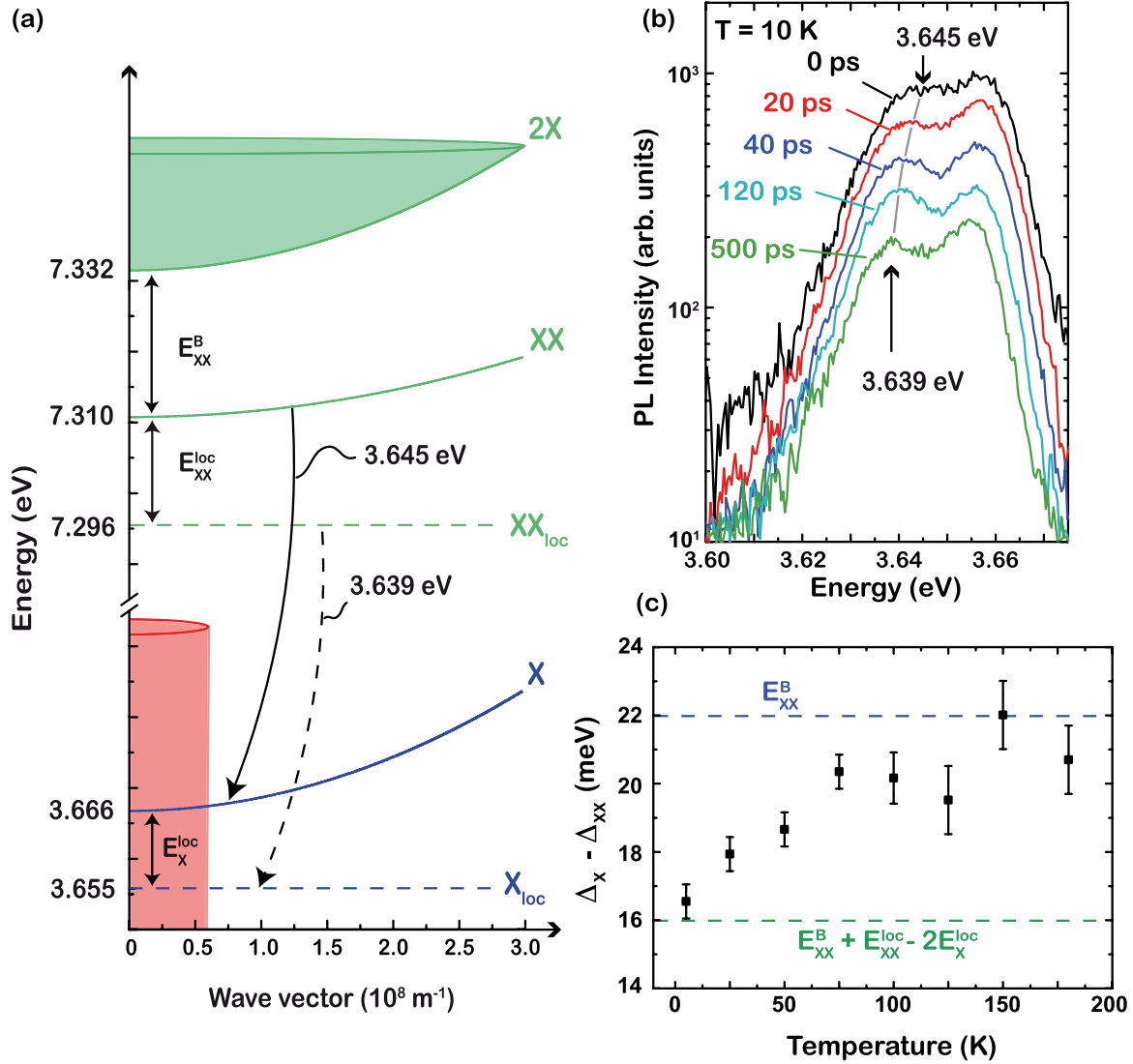


FIG. 3. (Color online) (a) In-plane dispersion of excitons ( $X$ ) and biexcitons ( $XX$ ) confined in an  $\text{Al}_{0.2}\text{Ga}_{0.8}\text{N}/\text{GaN}$  QW. Due to the conservation of the in-plane momentum, only excitons lying within the light cone (red) can couple to the light. Biexcitons form from the binding of two excitons ( $2X$ ). The energy difference between the bottom of the two-exciton continuum and a biexciton with zero-kinetic energy is equal to the biexciton binding energy  $E_{XX}^B$ . At 10 K, excitons and biexcitons are localized along the QW plane, with respective localization energy  $E_X^{\text{loc}}$  and  $E_{XX}^{\text{loc}}$ . (b) Time evolution of the MQW PL after nonresonant excitation. At zero delay, the biexciton emission is centered at 3.645 eV. It then redshifts and reaches 3.639 eV after 500 ps. For longer delays, the biexciton emission energy remains constant. This redshift provides a direct observation of the trapping of free biexcitons by potential fluctuations. (c) Temperature dependence of the energy difference between exciton and biexciton PL lines. At 10 K, excitons and biexcitons are localized, and their emission energy difference is given by  $\Delta_X - \Delta_{XX} = E_{XX}^B + E_{XX}^{\text{loc}} - 2E_X^{\text{loc}} = 16$  meV. When the temperature is increased, the energy difference between exciton and biexciton emissions evolves, due to their delocalization along the QW plane. At 200 K, excitons and biexcitons are fully delocalized, and we extract  $\Delta_X - \Delta_{XX} = E_{XX}^B = 22$  meV.

302 for the biexciton emission energy  $\Delta_{XX}$ :

$$\begin{aligned}
 \Delta_{XX} &= (2E_X - E_{XX}^B - E_{XX}^{\text{loc}}) - (E_X - E_X^{\text{loc}}) \\
 &= E_X + E_X^{\text{loc}} - E_{XX}^{\text{loc}} - E_{XX}^B,
 \end{aligned} \quad (2)$$

303 where  $E_{XX}^B$  is the biexciton binding energy. Since the re-  
 304 combination of a localized biexciton leaves an exciton that  
 305 is localized on the same site,<sup>44</sup> the energy difference at low  
 306 temperature between exciton and biexciton emissions is given  
 307 by:

$$\Delta_X - \Delta_{XX} = E_{XX}^B + E_{XX}^{\text{loc}} - 2E_X^{\text{loc}}. \quad (3)$$

With increasing temperature, excitons and biexcitons get  
 delocalized over the whole QW plane, and one gets back to the  
 usual relation for the difference between exciton and biexciton  
 emission energies:

$$\Delta_X - \Delta_{XX} = E_{XX}^B. \quad (4)$$

Experimentally, we observe that the energy difference  
 between exciton and biexciton emissions goes from 16 meV  
 at 10 K to 22 meV at 200 K [Fig. 3(c)]. Assuming that  
 excitons and biexcitons are delocalized at 200 K, we deduce  
 $E_{XX}^B = 22$  meV and  $E_{XX}^{\text{loc}} = 16$  meV (we verify *a posteriori*

317 that these binding and localization energies are consistent with  
 318 exciton and biexciton populations that are mostly delocalized  
 319 at 200 K—see Appendix). Since we estimate by envelope  
 320 function calculations the exciton binding energy to be 43 meV  
 321 (Fig. 1), we get  $E_{XX}^B/E_X^B = 0.51$ . Consequently, not only in  
 322 bulk ternary alloy<sup>42</sup> but also in QWs, disorder leads to a  
 323 deviation from the Haynes rule for the binding energy of  
 324 the biexciton.<sup>45</sup> In addition, from the biexciton binding and  
 325 localization energies determined above, we deduce that, at  
 326 10 K, free and localized QW biexciton emissions should lie  
 327 at 3.645 and 3.639 eV, respectively. Figure 3(b) shows the  
 328 low-temperature time evolution of QW exciton and biexciton  
 329 PL after nonresonant excitation. Just after the excitation,  
 330 the biexciton emission is centered, indeed, at 3.645 eV. It  
 331 then redshifts, reaching 3.639 eV after 500 ps, and then  
 332 its position remains constant for longer delays. Similarly to  
 333 what was observed for excitons confined in GaAs QWs with  
 334 single-monolayer well-width fluctuations,<sup>46</sup> this dynamical  
 335 redshift provides a direct observation of the trapping of free  
 336 biexcitons by potential fluctuations along the QW plane.

#### 337 IV. OPTICAL CHARACTERIZATION OF THE MQW 338 MC SAMPLE

##### 339 A. Emission properties of excitons in the MQW MC

340 We now turn our attention to the relaxation dynamics of  
 341 exciton polaritons in the MQW MC sample. The MC structure  
 342 features a cavity mode with a quality factor  $Q \sim 1000$ <sup>15</sup>  
 343 coupled with  $N = 67$  independent QW excitons. In *ideal*  
 344 samples, i.e., in absence of disorder and for fully coupled  
 345 QWs, the system, operating in the SCR, is described by  $N +$   
 346 1 eigenstates: two bright modes, the LPs and UPs, and  $N - 1$   
 347 exciton modes not coupled to the light, the dark excitons.<sup>20</sup>  
 348 We wish to emphasize that those dark excitons are not dark  
 349 from spin arguments, but only result from the diagonalization  
 350 of the Hamiltonian describing the interaction between a cavity  
 351 mode with  $N$  exciton states. Although necessarily present, we  
 352 will disregard, from now on, the role played by excitons with

353 a total angular momentum  $J = 2$ , as well as that of biexcitons  
 354 made out of  $J = 2$  excitons, in the overall relaxation scheme.<sup>48</sup>

355 The interest in working with such MQW MC arises  
 356 naturally from the fact that

357 (i) the exciton binding energy in (narrow polar) QWs is  
 358 increased compared to the bulk case<sup>36,47</sup> by a factor roughly  
 359 equal to 2,

360 (ii) the vacuum Rabi splitting scales with the square root  
 361 of the effective number  $N_{\text{eff}}$  of QWs inserted in the cavity.<sup>49</sup>  
 362 Note, however, that due to the homogeneous distribution of  
 363 QW over the full active region in our sample,  $N_{\text{eff}} \sim 33.5$ .  
 364 This means that half of the QWs do not participate in the  
 365 strong light-matter interaction with the external vacuum field  
 366 and act as a source of losses for the system,

367 (iii) the threshold power density is expected to be decreased  
 368 by a factor of 10 compared to the bulk case due to modified  
 369 matrix elements for the exciton-exciton interaction,<sup>50</sup> while the  
 370 exciton saturation density is increased owing to the decrease  
 371 in the exciton Bohr radius.

372 The far-field emission pattern at 10 K after nonresonant cw  
 373 excitation is shown in Figs. 4(a) and 4(b) for two different  
 374  $\delta$  values. In both cases, the MC is operating in the SCR, as  
 375 evidenced by the dispersion of the lower emission mode, which  
 376 we attribute to LPs. Now, the extracted occupancy of the LPB  
 377 displayed in Fig. 4(c) evidences that when going from slightly  
 378 positive to very negative  $\delta$  values, the occupancy of the bottom  
 379 of the LPB decreases [Fig. 4(c)]. For negative  $\delta$  values, the  
 380 energy relaxation of LPs is indeed hindered, due to the more  
 381 pronounced photon-like character of LPs, and their distribution  
 382 in  $k$ -space is far from thermal equilibrium. This relaxation  
 383 bottleneck is directly evidenced by the fact that the most  
 384 salient contribution to the emission arises from high- $k_{\parallel}$  states  
 385 [Fig. 4(a)]: the so-called exciton reservoir.<sup>6</sup> This bottleneck can  
 386 be overcome either by increasing the carrier density to favor  
 387 polariton-polariton interactions or by increasing the tempera-  
 388 ture to favor polariton-phonon interactions or finally by tuning  
 389 the cavity positively,<sup>10</sup> as the total scattering rate of polaritons  
 390 scales with the excitonic fraction in their wave function.

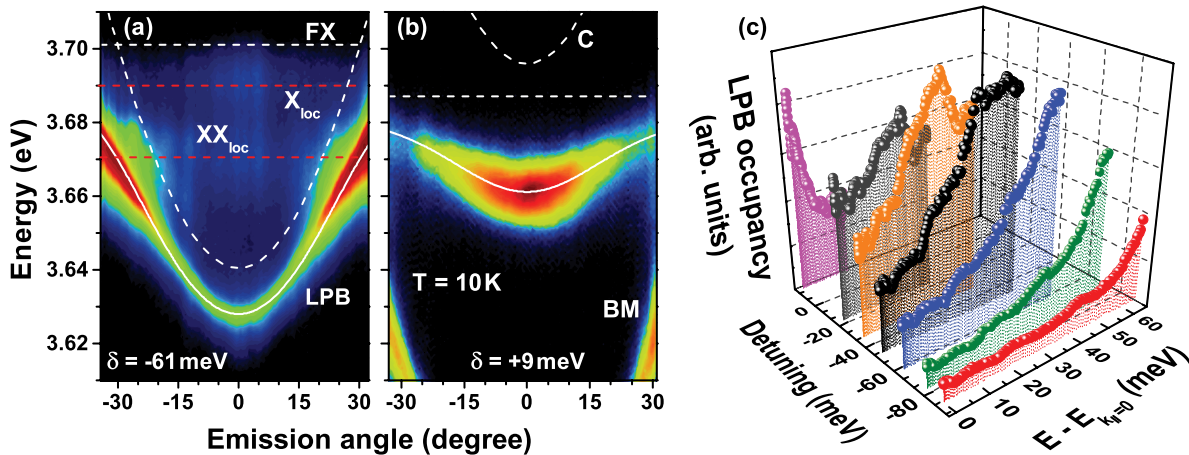


FIG. 4. (Color online) Angle-resolved PL spectra for a detuning (a)  $\delta = -61$  meV and (b)  $\delta = 9$  meV (arbitrary logarithmic color scale). The spectra have been taken with a cw frequency-doubled  $\text{Ar}^+$  laser ( $\lambda = 244$  nm) with an excitation power density of  $75 \text{ W/cm}^2$ . The white solid lines mark the dispersion of the LPB, while the white dashed lines show the uncoupled cavity (C) and FX modes. For negative  $\delta$  values the localized exciton and biexciton states are well resolved [red (dark gray) dashed lines], whereas for positive  $\delta$  values a leakage through a Bragg mode (BM) appears. (c) LPB occupancy evolution as a function of  $\delta$ .

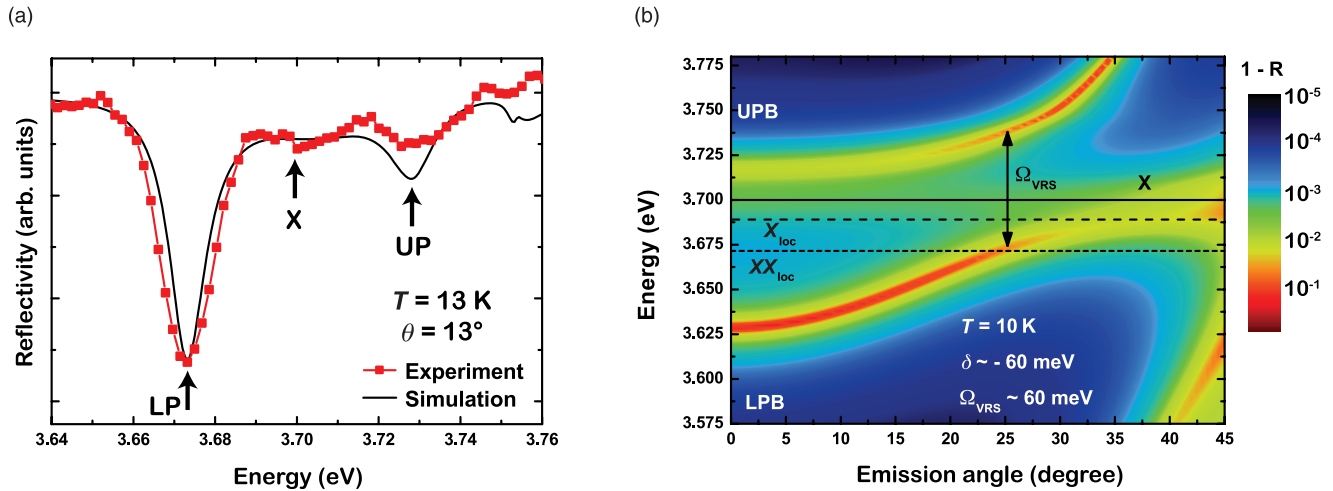


FIG. 5. (Color online) (a) Computed (black solid line) and measured (red symbols) reflectivity spectra of a GaN MQW MC at 13 K taken at an angle of  $13^\circ$ . LP, X, and UP point out the resonances of lower polaritons, free excitons, and upper polaritons, respectively. (b) computed angle resolved reflectivity ( $R$ ) spectra of a GaN MQW-MC at 10 K for a vacuum Rabi splitting  $\Omega_{\text{VRS}} = 60$  meV and a cavity detuning  $\delta = -60$  meV. The 67 QW exciton modes have been modeled by 67 independent and inhomogeneously broadened oscillators, giving rise to an optical signature at the energy of the uncoupled exciton. Note that  $1-R$  is displayed in logarithmic scale in order to enhance the visibility of the modes. UPB and LPB denote the UP and LP branches, respectively. Solid, dashed, and short-dash lines show the energy of FXs, localized excitons, and localized biexcitons, respectively.

391 In the specific case where  $\delta = -61$  meV, the LP PL at  
 392  $\mathbf{k}_{\parallel} = 0$  lies at 3.629 eV at 10 K. From the fitting of the LP PL  
 393 dispersion considering a vacuum Rabi splitting  $\Omega \sim 60$  meV,  
 394 as determined by previous reflectivity and PL experiments,<sup>15,16</sup>  
 395 we deduce that the uncoupled exciton and the bottom of the  
 396 UP branch (UPB) lie at 3.701 and 3.713 eV, respectively  
 397 [see Fig. 5(b)]. In addition to the PL from LPs, we observe  
 398 two emission lines at 3.671 and 3.690 eV. These lines are  
 399 dispersionless and correspond in energy neither to the UPB  
 400 nor to the uncoupled free QW exciton. The origin of those two  
 401 modes will be highlighted in the remaining part of this section  
 402 and the following one, while we describe in Sec. IV C their  
 403 role in the overall relaxation of LPs in the present MQW MC.

404 In *real* samples, nonidealities including alloy disorder, QW  
 405 width fluctuations, or even defects lead to a sharing of the  
 406 oscillator strength between the polariton modes and the dark  
 407 excitons.<sup>20</sup> Even if the SCR is preserved, dark excitons may  
 408 thus exhibit an optical signature in absorption, reflectivity, or  
 409 PL experiments.<sup>26</sup> On top of this an additional nonideality  
 410 comes into play for the present structure: QWs located apart  
 411 from the electric field antinodes are partly uncoupled from  
 412 the photonic cavity mode and are therefore adding an extra  
 413 contribution to the optical response. The combination of both  
 414 effects is responsible for the weak dip observed at the energy of  
 415 the uncoupled exciton mode in reflectivity measurements [cf.  
 416 Fig. 5(a)]. This measurement is in agreement with the results  
 417 of transfer matrix simulations shown in Fig. 5(b).

418 Similarly to what happens for excitons in the bare active  
 419 medium sample, uncoupled excitons in the full MC efficiently  
 420 localize on potential fluctuations distributed along the QW  
 421 planes. As the MQW and the MC samples have been grown  
 422 during the same run, the potential fluctuations along the QW  
 423 planes are likely to be the same in both samples leading us  
 424 to assume an exciton localization energy of  $\sim 11$  meV in  
 425 both cases.<sup>51</sup> Coming back to the experiments displayed in

Fig. 4, where the uncoupled exciton energy lies at 3.701 eV, we  
 deduce that the corresponding emission energy for localized  
 excitons is 3.690 eV: we consequently attribute the nondis-  
 persive transition detected at 3.690 eV to the recombination of  
 excitons localized along the QW planes.

## B. Cavity biexcitons

In order to reach a deeper understanding of the origin of the  
 3.671 eV line, we study, hereafter, its emission intensity decay  
 at normal incidence after nonresonant picosecond excitation,  
 together with the one of the localized exciton emission. While  
 the emission from localized excitons decays nonexponentially,  
 the line at 3.671 eV decays exponentially with a decay time  
 $\tau_{XX} = 335$  ps (Fig. 6). After  $\sim 795$  ps of decay, we observe that  
 the emission intensity decay of the 3.671 eV line quadratically  
 follows that of excitons. Similarly to the case of the bare-MQW  
 sample [Fig. 2(d)], this characteristic PL decay allows us to  
 attribute the line at 3.671 eV to the radiative dissociation of  
 cavity biexcitons (see Ref. 38 and Appendix). As discussed  
 theoretically in Ref. 20, dark excitons in MQW MCs efficiently  
 bind into biexcitons. These biexcitons then recombine and  
 leave either a dark exciton, a LP or an UP. It is important  
 to notice that for each of these recombination channels, the  
 photon leaving the cavity presents a different energy:

(i) first, a cavity biexciton can dissociate into a photon and  
 a dark exciton. The corresponding biexciton emission energy  
 is then nothing but  $\Delta_{XX} = E_X - E_{XX}^B$  for free biexcitons,  
 or  $\Delta_{XX} = E_X + E_X^{\text{loc}} - E_{XX}^{\text{loc}} - E_{XX}^B$  when biexcitons are  
 localized. Note that the equality sign might not hold exactly  
 as the MC biexciton binding energy was shown to be slightly  
 modified by the light-matter interaction,<sup>23</sup>

(ii) the radiative dissociation of a cavity biexciton can  
 also directly feed the LPB. Neglecting the dispersion of  
 biexcitons, we get that the biexciton emission energy is

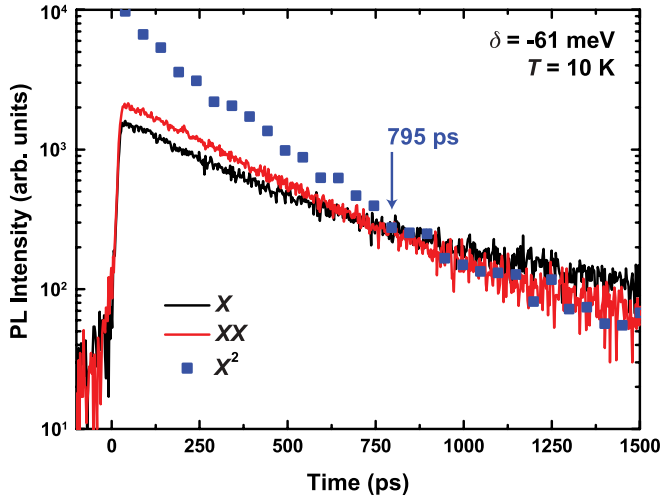


FIG. 6. (Color online) PL decays measured at 10 K for the exciton emission (black) and for the line at 3.671 eV [red (dark gray)], for a cavity detuning of  $-61$  meV. After 795 ps, the time-dependent emission intensity of the line centered at 3.671 eV follows the square of that of the exciton (blue symbols), evidencing its biexcitonic origin.

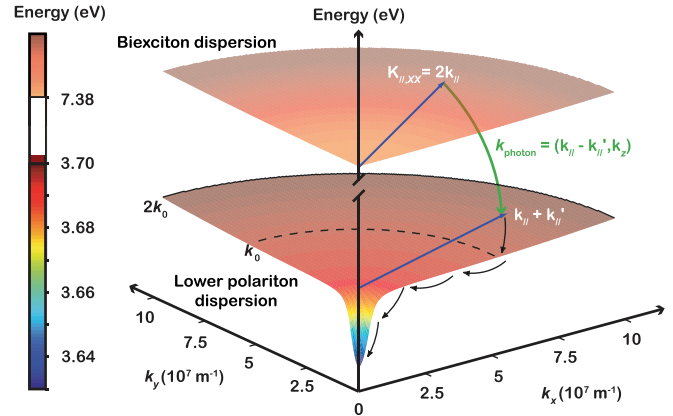


FIG. 7. (Color online) In-plane energy dispersion for LPs and biexcitons in the GaN MQW-MC for a detuning of  $-61$  meV between the cavity and the exciton modes. At negative detuning, the anticrossing behavior between the LP and UP eigenmodes generates a trap for the LPs with very low effective mass at the center of the Brillouin zone. Cavity biexcitons are formed from the binding of two dark excitons. Cavity biexcitons with an in-plane wave vector  $\mathbf{K}_{\parallel,XX}$  smaller than two times  $k_0 = nE_X(0)/\hbar c$  can efficiently couple to the light, where  $c$  denotes the speed of light and  $n$  is the optical refractive index. When a cavity biexciton recombines [green (medium gray) arrow], a photon and an LP are created, whose wave vectors must verify the conservation of the in-plane momentum. LPs then relax toward the center of the Brillouin zone through the emission of acoustic phonons (dark arrows).

radiative decay time of the order of the picosecond (see Fig. 7 and Ref. 6).

### C. Biexciton-assisted polariton relaxation

So far, we have described the available recombination channels for excitons, biexcitons, and polaritons. However, the relative relaxation rates of the different paths available are still unknown. It therefore does not allow us to apprehend which phenomenon is the one limiting the relaxation of polaritons toward the  $\mathbf{k}_{\parallel} = 0$  state and what is the role of the biexcitons in the polariton condensate formation. To solve this issue, we investigate in this section the evolution of the emission intensities and decay times of the different transitions with respect to the cavity detuning, and we finally measure the  $\delta$  dependence of the polariton lasing threshold. We first display in Fig. 8(a) the evolution of the emission spectra at small angles and after picosecond nonresonant excitation, for cavity detunings ranging from  $-40$  to  $-160$  meV. In addition to the emission from excitons, biexcitons, and LPs, other lines are observed. First, we observe at  $\sim 3.82$  eV a broad emission line that we attribute to the  $\text{Al}_{0.2}\text{Ga}_{0.8}\text{N}$  barrier [Fig. 8(b)]. We also detect two transitions that fall exactly, independent of the detuning, 91 meV below the exciton and biexciton emission lines. We thus ascribe these two lines to the exciton and cavity biexciton first LO-phonon replica, respectively. Finally, we observe between 3.3 and 3.5 eV several emission lines that, owing to their characteristic energy dispersion, we relate to leakage through Bragg modes.

$\Delta_{XX} = 2E_X - E_{XX}^B - E_{LP}(\mathbf{k}_{\parallel}^{LP}) > E_X - E_{XX}^B$ , where  $\mathbf{k}_{\parallel}^{LP}$  is the in-plane wave vector of the remaining LP,

(iii) finally, the recombination of a biexciton may also leave an UP. Then, the biexciton emission energy is  $\Delta_{XX} = 2E_X - E_{XX}^B - E_{UP}(\mathbf{k}_{\parallel}^{UP}) < E_X - E_{XX}^B$ , where  $\mathbf{k}_{\parallel}^{UP}$  is the in-plane wave vector of the remaining UP. We can already note that, in our case, the biexciton emission lies at much too high energy to be ascribed to this recombination channel.

Contrary to excitons, which are dark when their kinetic energy exceeds 0.1 meV,<sup>52,53</sup> biexcitons can couple to light, whatever their in-plane wave vector.<sup>54</sup> This arises from the fact that even if the recombination of a biexciton requires momentum conservation, the remaining wave vector is transferred to the exciton or to the polariton left after the radiative dissociation (Fig. 7). As a consequence, regarding the distributions of excitons and biexcitons in  $k$ -space compared to the limited extension of the trap formed by LPs (see Fig. 7), the most probable channels for the recombination of cavity biexcitons are those leaving either an exciton or LP in the reservoir, i.e., at high in-plane momentum beyond the LPB inflection point. It is important to notice here that, as shown by the transfer matrix simulations displayed in Fig. 5(b), 1-R does not strictly go to zero at the emission energy of excitons and biexcitons, meaning that the photons resulting from the recombination of excitons and biexcitons can easily leak out from the cavity. The finite broadening of both the exciton and the cavity modes also increases the density of states available for the radiative dissociation of a given biexciton state, therefore increasing its recombination probability compared to the ideal case treated in Ref. 20. Finally, while uncoupled excitons accumulate, get localized, and then recombine, LPs accumulate in the reservoir. In the low excitation density regime, the latter lose their excess of kinetic energy via interactions with the surrounding electronic population and with acoustic phonons, they relax toward the bottom of the LPB and finally escape from the cavity with a



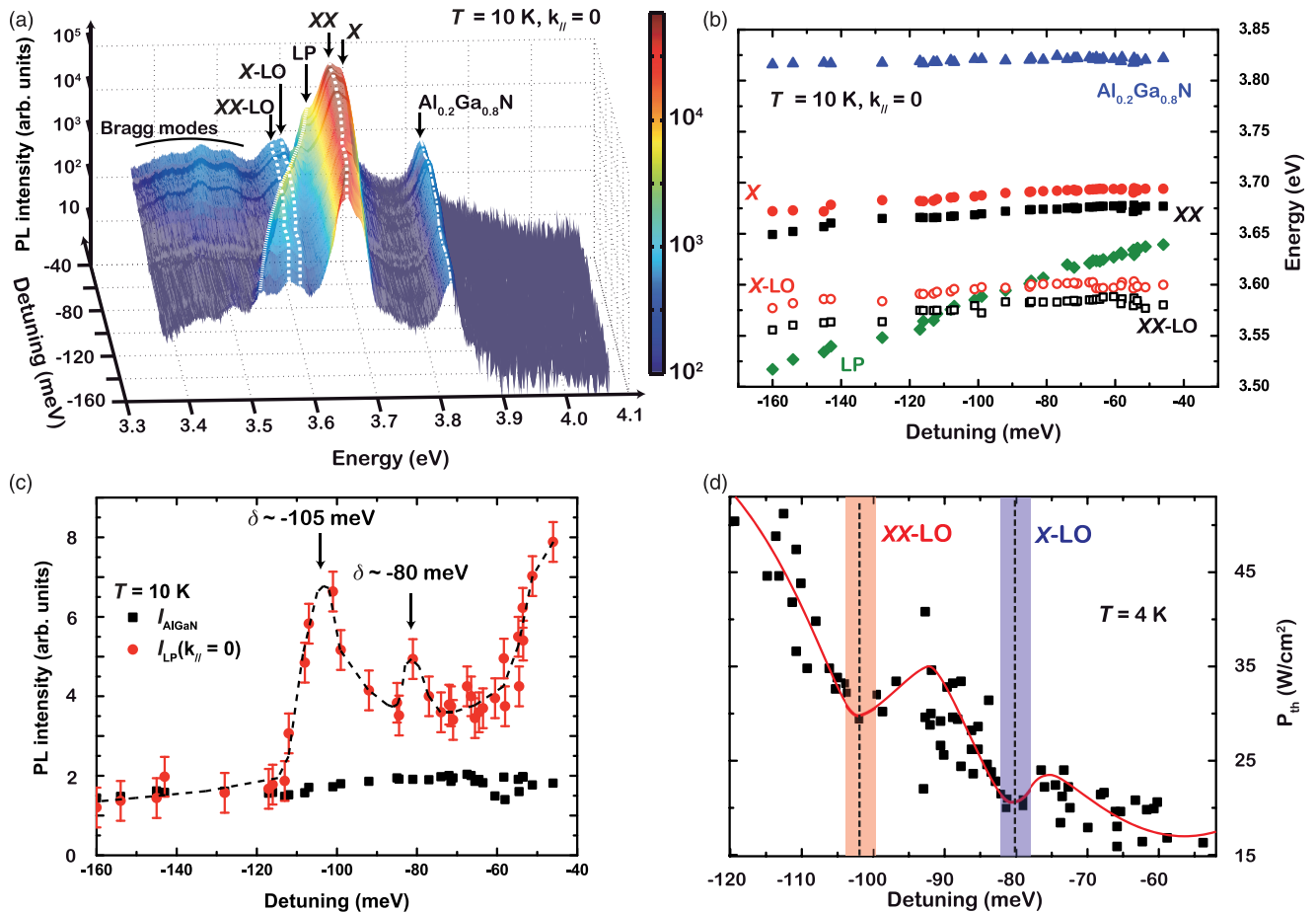


FIG. 8. (Color online) (a) TI PL spectra of the GaN MQW MC taken under nonresonant excitation, at normal incidence at 10 K, with respect to the cavity detuning ( $\delta$ ). White lines are guides to the eye showing the  $\delta$  dependence of biexciton ( $XX$ ), exciton, and biexciton first LO-phonon replica ( $X$ -LO and  $XX$ -LO, respectively), bottom of the LPB (LP) and  $Al_{0.2}Ga_{0.8}N$  emission energies. (b)  $Al_{0.2}Ga_{0.8}N$ ,  $X$ ,  $XX$ , LP,  $X$ -LO, and  $XX$ -LO emission energies with respect to  $\delta$ . When  $\delta = -80$  and  $-105$  meV, LP corresponds in energy to  $X$ -LO and  $XX$ -LO, respectively. (c) Emission intensity from the (Al,Ga)N (squares) and the bottom of the LPB (circles) measured at 10 K versus  $\delta$ . The emission intensities from LP and  $Al_{0.2}Ga_{0.8}N$  have been obtained after a careful deconvolution of the TI PL spectra displayed in (a). (d) Polariton lasing threshold power density ( $P_{th}$ ) measured at 4 K under nonresonant pumping with a Nd:YAG laser as a function of  $\delta$ . Two local minima in  $P_{th}$  are observed when  $\delta = -80$  and  $-105$  meV. In (c) and (d), lines are guides for the eyes.

When going from a cavity detuning of  $-40$  to  $-160$  meV, keeping the excitation power density constant, we only observe slight variations in the (Al,Ga)N emission intensity, indicating that the injected carrier density has been kept almost constant for all experiments [Fig. 8(c)]. Moreover, although the emission energy of excitons and biexcitons fluctuates when varying  $\delta$  [the exciton emission energy goes from 3.652 to 3.695 eV, when  $\delta$  is tuned between  $-160$  and  $-40$  meV, see Fig. 8(b)], due to strain variation along the wedge of the sample, their energy separation is always kept equal to  $19 \pm 1$  meV. We underline also that, for all  $\delta$  values, the time-decay of the biexciton emission follows quadratically that of the exciton emission after  $\sim 700 - 900$  ps (Fig. 9), evidencing that the discussion developed in Secs. III A and III B for  $\delta = -61$  meV can be readily extended to the whole range  $-40 < \delta < -160$  meV.

Now, in contrast to exciton and biexciton emission lines, the emission intensity from LPs at  $k_{\parallel} = 0$  shows strong variations with respect to  $\delta$  [Fig. 8(c)]. First, for  $\delta$  comprised

between  $-40$  and  $-70$  meV and for  $\delta < -110$  meV, we observe a decrease in the emission intensity of LPs at  $k_{\parallel} = 0$ , when  $\delta$  is reduced. This decrease in emission intensity at normal incidence for LPs arises from the fact that, when going from slightly to very negative detunings, the scattering rate of LPs with acoustic phonons decreases owing to the increasing photonic character of the polaritons, hampering the polariton relaxation toward the Brillouin zone center.<sup>6</sup> Polaritons in the reservoir are therefore more likely to escape from the cavity through leaky modes (or to recombine nonradiatively) than to relax down to the bottom of the branch. Superimposed to this general trend, two local maxima for the emission intensity of LPs at  $k_{\parallel} = 0$  are observed. The first one occurs when  $\delta = -80$  meV, i.e., when the energy of LP( $k_{\parallel} = 0$ ) corresponds to that of the first LO-phonon replica of the exciton. This behavior is similar to that first reported by Boeuf *et al.* for CdTe MCs, where a local minimum in the polariton lasing threshold was observed, when the energy difference between the bottom of the LPB and the excitonic reservoir matches the energy of

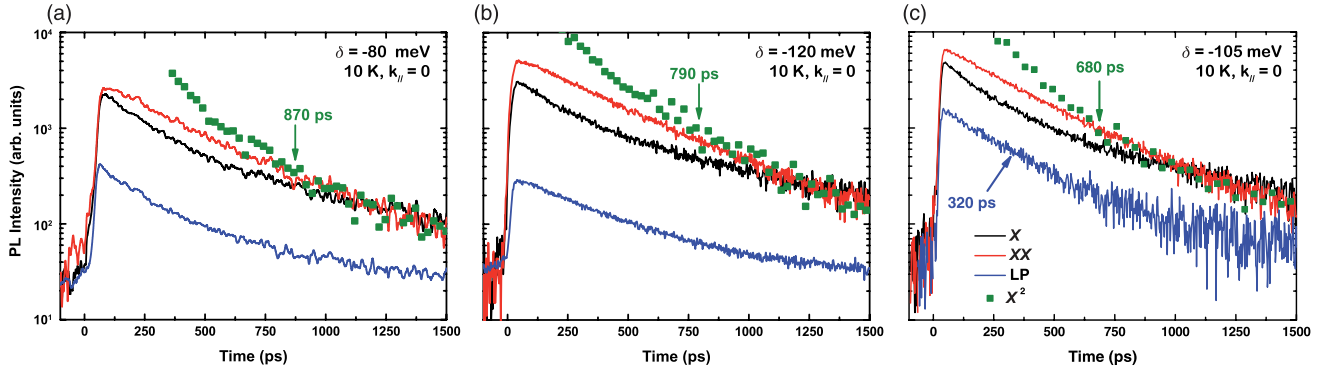


FIG. 9. (Color online) Low-temperature PL decays for the exciton (black), biexciton [red (dark gray)], and LP [blue (medium gray)] emissions at  $\mathbf{k}_{\parallel} = 0$ , for a detuning  $\delta = -80$  (a),  $-120$  (b), and  $-105$  meV (c). In (a) and (b), the LP emission follows the same dynamics as the exciton. On the contrary, when  $\delta = -105$  meV (c), both the biexciton and the LP emissions exponentially decay with a decay time of 320 ps. For all detunings, the biexciton emission intensity follows the square of that of the exciton (green symbols) after  $\sim 700$ – $900$  ps, evidencing full thermalization between exciton and biexciton states.

one LO-phonon.<sup>55</sup> In our case, the local increase in the PL intensity of LP( $\mathbf{k}_{\parallel} = 0$ ) evidences the efficient LO-phonon assisted transfer of both uncoupled excitons and high- $\mathbf{k}_{\parallel}$  LPs to the bottom of the LPB. A second local maximum is observed for  $\delta \sim -105$  meV, when the bottom of the LPB corresponds in energy to that of the first LO-phonon replica of the biexciton. In the same way, we attribute this observation to the direct feeding of  $\mathbf{k}_{\parallel} = 0$  LP states by the radiative dissociation of cavity biexcitons assisted by one LO-phonon. In other words, the processes “ $XX \rightarrow \text{LP}(\mathbf{k}_{\parallel} = 0) + \text{LO} + X$ ” and “ $XX \rightarrow \text{LP}(\mathbf{k}_{\parallel} = 0) + \text{LO} + \text{LP}(\text{high-}\mathbf{k}_{\parallel})$ ” provide efficient ways of relaxation toward the bottom of the LPB. If we now monitor the evolution with  $\delta$  of the polariton condensation threshold under nonresonant optical pumping at 4 K, we observe two minima for  $\delta = -80$  and  $-105$  meV [Fig. 8(d)]. Similarly to Refs. 55–57, we attribute the former minimum to the relaxation of exciton in the reservoir by the emission of one LO-phonon, allowing for bypassing the relaxation bottleneck. Regarding the second minimum polariton lasing threshold lying at  $\delta = -105$  meV, it corresponds to the case where LP( $\mathbf{k}_{\parallel} = 0$ ) arise from the LO-phonon-assisted radiative dissociation of cavity biexcitons.

To further support our view, we display in Fig. 9 the decay of the luminescence from LP( $\mathbf{k}_{\parallel} = 0$ ) for various  $\delta$  values. For  $\delta$  comprised between  $-40$  and  $-95$  meV and between  $-110$  and  $-160$  meV, we observe that the LP PL at normal incidence decays nonexponentially and follows at all times the same dynamics as the exciton PL [Figs. 9(a) and 9(b)]. This behavior demonstrates (i) that the uncoupled exciton branches are at thermal equilibrium with the LP reservoir and (ii) that the decay of the reservoir itself is limited by LP-LP and LP-acoustic phonons scattering. In other words, the PL decay of the bottom of the LPB is imposed by the relaxation of LPs from the reservoir to the trap.<sup>58</sup> Of course, in the specific case where  $\delta = -80$  meV, and in agreement with the previous discussion, the relaxation of excitons and LPs in the reservoir is dominated by their scattering with LO-phonons rather than with acoustic phonons. On the contrary, when  $\delta \sim -105$  meV, LPs at  $\mathbf{k}_{\parallel} = 0$  and biexcitons both decay exponentially with a decay time of 320 ps [Fig. 9(c)]. In the latter situation, and in agreement with the data displayed in Figs. 8(c) and 8(d), the feeding of the

$\mathbf{k}_{\parallel} = 0$  LPs states is then dominated by the radiative dissociation of cavity biexcitons.

A deeper understanding of the role played by biexcitons in semiconductor MCs operating in the SCR is of special interest as they strongly interact with the polariton population. Under coherent (resonant) excitation, the presence of biexcitons can significantly alter the light-matter coupling. As already mentioned, with increasing pump intensity, a progressive transfer of oscillator strength from the exciton to the biexciton transition was evidenced by pump-probe experiments, favoring the formation of biexciton polaritons to the detriment of exciton polaritons.<sup>24</sup> More recently, the progressive formation of biexcitons from two excitons of opposite spins has been shown to hinder the light-matter coupling through the introduction of nonlinear losses, favoring a given spin population at the expense of the other one.<sup>59</sup> Biexcitons should be thus included in the description of the relaxation in QW-based MCs in order to complete the picture of the interactions occurring within the polariton ensemble. This particularly affects the renormalization of the polariton dispersion. In the usual framework, only polariton-exciton and polariton-polariton interactions are considered resulting in a linear scaling of the polariton ground-state energy with its population—below and above the condensation threshold. This behavior is described by the two interaction constants:  $\alpha_1 > 0$ , describing the repulsive interaction between polaritons with the same spin and  $\alpha_2 < 0$ , the attractive interaction between polaritons with opposite spin.<sup>60</sup> It is generally assumed that  $|\alpha_2| \ll \alpha_1$ , due to the dominating contribution of the exchange interaction term in two-dimensional systems.<sup>61</sup> It was shown that the biexciton-mediated interaction results in an effective polariton-polariton attraction that strongly affects the sign and strength of  $\alpha_2$ <sup>62,63</sup> and can increase the efficiency of the LP-LP scattering processes due to the appearance of the singlet biexciton state as an intermediate transition.<sup>64</sup> Interestingly, depending on the detuning, the ratio  $\alpha_2/\alpha_1$  can eventually go below  $-1$ , i.e., the attraction overcomes the repulsion, making possible the coexistence of condensation in real and reciprocal spaces.<sup>63</sup> We believe that, thanks to the large biexciton binding energy in GaN QWs, III-nitride based MCs are prototypical systems to gain a deeper understanding

642 of the biexciton contribution to the  $\alpha_1$  and  $\alpha_2$  coefficients.  
 643 This will not only allow for a better comprehension of  
 644 the polariton branch renormalization and the overall relax-  
 645 ation dynamics, but this can also offer a better tuning of  
 646 polariton spin-dependent devices such as ultrafast optical spin  
 647 switches.<sup>65</sup>

## 648 V. CONCLUSION

649 In summary, the radiative dissociation of biexcitons in  
 650 a MQW III-nitride based MC operating in the SCR has  
 651 been investigated by means of continuous wave and TR  
 652 PL techniques. The direct observation of cavity biexciton  
 653 emission has been facilitated by the nonidealities of the  
 654 cavity active medium, which lead to a redistribution of the  
 655 oscillator strength between the polariton states and the dark  
 656 QW excitons. When the energy of the bottom of the LPB  
 657 corresponds to that of the first LO-phonon replica of the cavity  
 658 biexciton, we observe an enhanced scattering of polaritons  
 659 toward the  $\mathbf{k}_{\parallel} = 0$  state, as well as a decrease in condensation  
 660 threshold. This fact, combined with the observation of identical  
 661 decay rates, evidences that, for this peculiar detuning, the  
 662 mechanism limiting the energy relaxation of polaritons is the  
 663 dissociation of cavity biexcitons into a LP, a LO phonon,  
 664 and an exciton, rather than the inelastic scattering of exciton-  
 665 polaritons with acoustic phonons. Our study clearly evidences  
 666 that biexcitons have to be taken into account when describing  
 667 the polariton relaxation in MCs, and we believe that it  
 668 will stimulate more work aiming at understanding the role  
 669 of multiexcitonic complexes on the formation of polariton  
 670 condensates.

## 671 ACKNOWLEDGMENTS

672 The authors would like to thank R. Rochat, N. Leiser,  
 673 D. Trolliet, and N. Trolliet for technical support. We acknowl-  
 674 edge the financial support from the NCCR Quantum Photonics,  
 675 research instrument of the Swiss National Science Foundation

through Grant No. 129715 and Grant No. 200020-113542, and  
 from the EU-project Clermont4 (Grant No. FP7-235114).

## 678 APPENDIX

679 We detail here the relations describing the equilibrium  
 680 between free and localized excitons and biexcitons in order  
 681 to show that in a thermalized system, the time dependence  
 682 of localized biexciton emission follows the square of the  
 683 time dependence of the localized exciton emission. For  
 684 completeness, we also account in our modeling for free  
 685 electron-hole pairs.

686 Using the expression given in Refs. 66 and 67, the thermal  
 687 dissociation of free QW excitons into free electron-hole pairs  
 688 writes:

$$\frac{N_e N_h}{N_X^{fr}} = \frac{\mu k T}{2\pi\hbar^2} \exp\left[-\frac{E_X^B}{kT}\right], \quad (\text{A1})$$

689 where  $N_e$ ,  $N_h$ , and  $N_X^{fr}$  are the densities of electrons, holes,  
 690 and FXs confined in the QW, respectively, and  $\mu$  is the exciton-  
 691 reduced mass. Similarly, Saha's law for FXs and biexcitons is  
 692 given by:

$$\frac{(N_X^{fr})^2}{N_{XX}^{fr}} = \frac{MkT}{\pi\hbar^2} \exp\left[-\frac{E_{XX}^B}{kT}\right], \quad (\text{A2})$$

693 where  $N_{XX}^{fr}$  is the biexciton density and  $M$  is the exciton  
 694 translational mass. In presence of disorder, QW excitons  
 695 localize due to interface roughness, and the thermal exchange  
 696 between localized and free QW excitons is described by:<sup>68</sup>

$$\frac{N_X^{fr}}{N_X^{loc}} = \frac{2MkT}{\pi\hbar^2 N_D} \exp\left[-\frac{E_X^{loc}}{kT}\right], \quad (\text{A3})$$

697 where  $N_X^{loc}$  is the density of localized excitons and  $N_D$  is the  
 698 density of localizing centers. As shown in the present paper,  
 699 biexcitons also efficiently localize along the QW plane. We  
 700 therefore readily extend Eq. (A3) to the equilibrium between

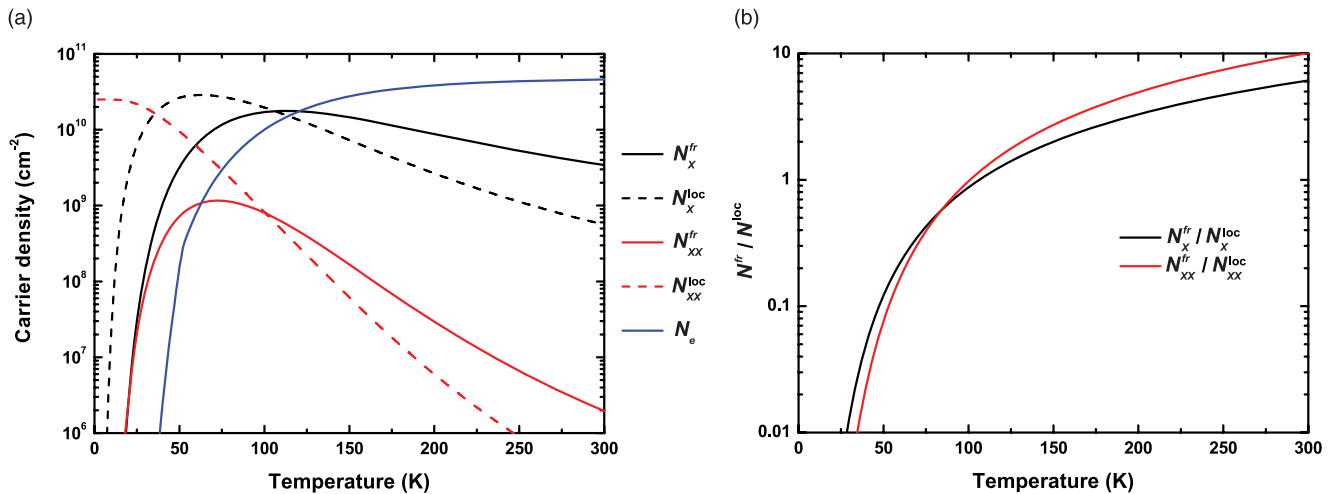


FIG. 10. (Color online) (a) Calculated-free (solid lines) and localized (dashed lines) densities of excitons, biexcitons, and electrons [black, red (dark gray), and blue (medium gray), respectively] confined in a 1.2-nm-thick Al<sub>0.2</sub>Ga<sub>0.8</sub>N/GaN QW for a photogenerated pair density of  $5 \times 10^{10} \text{ cm}^{-2}$ . (b) Ratios between free and localized exciton (black) and biexciton [red (dark gray)] densities with respect to temperature. At 200 K, excitons and biexcitons are mainly delocalized along the QW plane.

701 localized and free biexcitons, yielding:

$$\frac{N_{XX}^{fr}}{N_{XX}^{loc}} = \frac{4MkT}{\pi\hbar^2 N_D} \exp\left[-\frac{E_{XX}^{loc}}{kT}\right], \quad (\text{A4})$$

702 where  $N_{XX}^{loc}$  is the density of localized biexcitons. In Eqs. (A3)  
703 and (A4), we have assumed that the same density of localizing  
704 centers was accessible for both excitons and biexcitons.  
705 Combining Eqs. (A2)–(A4) then leads to:

$$\frac{(N_X^{loc})^2}{N_{XX}^{loc}} = N_D \exp\left[-\frac{E_{XX}^B + E_{XX}^{loc} - 2E_X^{loc}}{kT}\right]. \quad (\text{A5})$$

706 The emission intensity for a distribution of excitons is pro-  
707 portional to the radiative part of its temporal derivative. There-

fore, in a thermalized system, the time-dependent emission  
708 intensity from localized biexcitons  $I_{XX}^{loc}(t)$  follows at all times  
709 the square of that of localized excitons  $I_X^{loc}(t)$ . Following the  
710 procedure described in Ref. 69, we can numerically calculate  
711 for all temperatures the densities of excitons, biexcitons, and  
712 free carriers confined in the QWs. In these calculations, we  
713 have taken  $E_X^B = 43$  meV (Fig. 1),  $E_X^{loc} = 11$  meV (Fig. 2),  
714 and  $E_{XX}^B = 22$  meV and  $E_{XX}^{loc} = 16$  meV (Fig. 3), and we have  
715 tentatively assumed that  $N_D = 3 \times 10^{12}$  cm<sup>-2</sup>, as determined  
716 previously in Ref. 53. In addition, as our layers are nominally  
717 undoped, we take  $N_e = N_h$ . The result of our calculations,  
718 displayed in Fig. 10 for a photogenerated carrier density  
719  $N_{tot} = 5 \times 10^{10}$  cm<sup>-2</sup>, verifies *a posteriori* that at 200 K,  
720 excitons and biexcitons are mostly delocalized. 721

\*Corresponding author: pmc53@cam.ac.uk

†Present address: Cavendish Laboratory, University of Cambridge,  
J. J. Thomson Avenue, Cambridge CB3 0HE, United Kingdom.

<sup>1</sup>C. Weisbuch, M. Nishioka, A. Ishikawa, and Y. Arakawa, *Phys. Rev. Lett.* **69**, 3314 (1992).

<sup>2</sup>P. G. Savvidis, J. J. Baumberg, R. M. Stevenson, M. S. Skolnick, D. M. Whittaker, and J. S. Roberts, *Phys. Rev. Lett.* **84**, 1547 (2000).

<sup>3</sup>J. Kasprzak, M. Richard, S. Kundermann, A. Baas, P. Jeambrun, J. M. J. Keeling, F. M. Marchetti, M. H. Szymanska, R. André, J. L. Staehli, V. Savona, P. B. Littlewood, B. Deveaud, and Le Si Dang, *Nature (London)* **443**, 409 (2006).

<sup>4</sup>S. Christopoulos, G. Baldassari Höger von Högersthal, A. J. D. Grundy, P. G. Lagoudakis, A. V. Kavokin, J. J. Baumberg, G. Christmann, R. Butté, E. Feltn, J.-F. Carlin, and N. Grandjean, *Phys. Rev. Lett.* **98**, 126405 (2007).

<sup>5</sup>A. Imamoglu, R. J. Ram, S. Pau, and Y. Yamamoto, *Phys. Rev. A* **53**, 4250 (1996).

<sup>6</sup>F. Tassone, C. Piermarocchi, V. Savona, A. Quattropani, and P. Schwendimann, *Phys. Rev. B* **56**, 7554 (1997).

<sup>7</sup>C. Ciuti, P. Schwendimann, B. Deveaud, and A. Quattropani, *Phys. Rev. B* **62**, R4825 (2000).

<sup>8</sup>Y. G. Rubo, G. Malpuech, A. V. Kavokin, and P. Bigenwald, *Phys. Rev. Lett.* **91**, 156403 (2003).

<sup>9</sup>R. Butté, G. Delalleau, A. I. Tartakovskii, M. S. Skolnick, V. N. Astratov, J. J. Baumberg, G. Malpuech, A. Di Carlo, A. V. Kavokin, and J. S. Roberts, *Phys. Rev. B* **65**, 205310 (2002).

<sup>10</sup>A. I. Tartakovskii, M. Emam-Ismael, R. M. Stevenson, M. S. Skolnick, V. N. Astratov, D. M. Whittaker, J. J. Baumberg, and J. S. Roberts, *Phys. Rev. B* **62**, R2283 (2000).

<sup>11</sup>J. Bloch, T. Freixanet, J.-Y. Marzin, V. Thierry-Mieg, and R. Planel, *Appl. Phys. Lett.* **73**, 1694 (1998).

<sup>12</sup>G. Malpuech, A. Kavokin, A. Di Carlo, and J. J. Baumberg, *Phys. Rev. B* **65**, 153310 (2002).

<sup>13</sup>E. Wertz, L. Ferrier, D. D. Solnyshkov, P. Senellart, D. Bajoni, A. Miard, A. Lemaître, G. Malpuech, and J. Bloch, *Appl. Phys. Lett.* **95**, 051108 (2009).

<sup>14</sup>J. Levrat, R. Butté, E. Feltn, J.-F. Carlin, N. Grandjean, D. Solnyshkov, and G. Malpuech, *Phys. Rev. B* **81**, 125305 (2010).

<sup>15</sup>G. Christmann, R. Butté, E. Feltn, A. Mouti, P. A. Stadelmann, A. Castiglia, J.-F. Carlin, and N. Grandjean, *Phys. Rev. B* **77**, 085310 (2008).

<sup>16</sup>G. Christmann, R. Butté, E. Feltn, J.-F. Carlin, and N. Grandjean, *Appl. Phys. Lett.* **93**, 051102 (2008).

<sup>17</sup>R. Butté, J. Levrat, G. Christmann, E. Feltn, J.-F. Carlin, and N. Grandjean, *Phys. Rev. B* **80**, 233301 (2009).

<sup>18</sup>D. M. Whittaker, P. Kinsler, T. A. Fisher, M. S. Skolnick, A. Armitage, A. M. Afshar, M. D. Sturge, and J. S. Roberts, *Phys. Rev. Lett.* **77**, 4792 (1996).

<sup>19</sup>V. Savona, C. Piermarocchi, A. Quattropani, F. Tassone, and P. Schwendimann, *Phys. Rev. Lett.* **78**, 4470 (1997).

<sup>20</sup>G. C. La Rocca, F. Bassani, and V. M. Agranovich, *J. Opt. Soc. Am. B* **15**, 652 (1998).

<sup>21</sup>M. Kuwata-Gonokami, S. Inouye, H. Suzuura, M. Shirane, R. Shimano, T. Someya, and H. Sakaki, *Phys. Rev. Lett.* **79**, 1341 (1997).

<sup>22</sup>X. Fan, H. Wang, H. Q. Hou, and B. E. Hammons, *Phys. Rev. B* **57**, R9451 (1998).

<sup>23</sup>P. Borri, W. Langbein, U. Woggon, A. Esser, J. R. Jensen, and J. M. Hvam, *Semicond. Sci. Technol.* **18**, S351 (2003).

<sup>24</sup>M. Saba, F. Quochi, C. Ciuti, U. Oesterle, J. L. Staehli, B. Deveaud, G. Bongiovanni, and A. Mura, *Phys. Rev. Lett.* **85**, 385 (2000).

<sup>25</sup>G. Christmann, D. Simeonov, R. Butté, E. Feltn, J.-F. Carlin, and N. Grandjean, *Appl. Phys. Lett.* **89**, 261101 (2006).

<sup>26</sup>R. Houdré, R. P. Stanley, and M. Ilegems, *Phys. Rev. A* **53**, 2711 (1996).

<sup>27</sup>F. Stokker-Cheregi, A. Vinattieri, E. Feltn, D. Simeonov, J.-F. Carlin, R. Butté, N. Grandjean, and M. Gurioli, *Phys. Rev. B* **77**, 125342 (2008).

<sup>28</sup>K. Okada, Y. Yamada, T. Taguchi, F. Sasaki, S. Kobayashi, T. Tani, S. Nakamura, and G.-I. Shinomiya, *Jpn. J. Appl. Phys.* **35**, L787 (1996).

<sup>29</sup>Y. Kawakami, Z. G. Peng, Y. Narukawa, S. Fujita, and S. Nakamura, *Appl. Phys. Lett.* **69**, 1414 (1996).

<sup>30</sup>S. Amloy, K. H. Yu, K. F. Karlsson, R. Farivar, T. G. Andersson, and P. O. Holtz, *Appl. Phys. Lett.* **99**, 251903 (2011).

<sup>31</sup>E. Feltn, D. Simeonov, J.-F. Carlin, R. Butté, and N. Grandjean, *Appl. Phys. Lett.* **90**, 021905 (2007).

<sup>32</sup>M. Leroux, N. Grandjean, J. Massies, B. Gil, P. Lefebvre, and P. Bigenwald, *Phys. Rev. B* **60**, 1496 (1999).

<sup>33</sup>J.-W. Wu, *Solid State Commun.* **67**, 911 (1988).

<sup>34</sup>R. Zimmermann and D. Bimberg, *Phys. Rev. B* **47**, 15789 (1993).

- <sup>35</sup>A. Bellabchara, P. Lefebvre, P. Christol and H. Mathieu, *Phys. Rev. B* **50**, 11840 (1994).
- <sup>36</sup>G. Bastard, E. E. Mendez, L. L. Chang, and L. Esaki, *Phys. Rev. B* **26**, 1974 (1982).
- <sup>37</sup>P. Lefebvre, S. Kalliakos, T. Bretagnon, P. Valvin, T. Taliercio, B. Gil, N. Grandjean, and J. Massies, *Phys. Rev. B* **69**, 035307 (2004).
- <sup>38</sup>J. C. Kim, D. R. Wake, and J. P. Wolfe, *Phys. Rev. B* **50**, 15099 (1994).
- <sup>39</sup>C. Weisbuch, R. Dingle, A. C. Gossard, and W. Wiegmann, *Solid State Commun.* **38**, 709 (1981).
- <sup>40</sup>F. Natali, Y. Cordier, J. Massies, S. Vezian, B. Damilano, and M. Leroux, *Phys. Rev. B* **79**, 035328 (2009).
- <sup>41</sup>Note that this value is higher than what was reported in the literature for (Al,Ga)N layers with similar Al-content, see, for instance, K. B. Lee, P. J. Parbrook, T. Wang, F. Ranalli, T. Martin, R. S. Balmer, and D. J. Wallis, *J. Appl. Phys.* **101**, 053513 (2007).
- <sup>42</sup>W. Langbein and J. M. Hvam, *Phys. Rev. B* **59**, 15405 (1999).
- <sup>43</sup>Y. Yamada, Y. Ueki, K. Nakamura, T. Taguchi, A. Ishibashi, Y. Kawaguchi, and T. Yokogawa, *Phys. Rev. B* **70**, 195210 (2004).
- <sup>44</sup>S. T. Cundiff, T. Zhang, A. D. Bristow, D. Karaiskaj, and X. Dai, *Acc. Chem. Res.* **42**, 1423 (2009).
- <sup>45</sup>D. Birkedal, J. Singh, V. G. Lyssenko, J. Erland, and J. M. Hvam, *Phys. Rev. Lett.* **76**, 672 (1996).
- <sup>46</sup>B. Deveaud, T. C. Damen, J. Shah, and C. W. Tu, *Appl. Phys. Lett.* **51**, 828 (1987).
- <sup>47</sup>Below the condensation threshold,  $J = 2$  excitons create a reservoir of dark excitons and dark biexcitons, which leads to an increase in radiative lifetime for both the exciton and biexciton populations. Above the condensation threshold, the presence of this dark reservoir slightly increases the energy of the polariton condensate, therefore contributing to the  $\alpha_2$  term discussed at the end of the paper.
- <sup>48</sup>N. Grandjean, B. Damilano, S. Dalmaso, M. Leroux, M. Läügt, and J. Massies, *J. Appl. Phys.* **86**, 3714 (1999).
- <sup>49</sup>V. Savona, L. C. Andreani, P. Schwendimann, and A. Quattropani, *Solid State Commun.* **93**, 733 (1995).
- <sup>50</sup>D. Solnyshkov, H. Ouerdane, and G. Malpuech, *J. Appl. Phys.* **103**, 016101 (2008).
- <sup>51</sup>Note that despite the present inhomogeneous broadening of 11 meV, the strong coupling regime is preserved as we measure a Rabi splitting of 60 meV.
- <sup>52</sup>L. C. Andreani, F. Tassone, and F. Bassani, *Solid State Commun.* **77**, 641 (1991).
- <sup>53</sup>P. Corfdir, J. Levrat, A. Dussaigne, P. Lefebvre, H. Teisseyre, I. Grzegory, T. Suski, J.-D. Ganière, N. Grandjean, and B. Deveaud-Plédran, *Phys. Rev. B* **83**, 245326 (2011).
- <sup>54</sup>D. S. Citrin, *Phys. Rev. B* **50**, 17655 (1994).
- <sup>55</sup>F. Boeuf, R. André, R. Romestain, Le Si Dang, E. Péronne, J.-F. Lampin, D. Hulin, and A. Alexandrou, *Phys. Rev. B* **62**, R2279 (2000).
- <sup>56</sup>M. Maragkou, A. J. D. Grundy, T. Ostatnicky, and P. G. Lagoudakis, *Appl. Phys. Lett.* **97**, 111110 (2010).
- <sup>57</sup>L. Orosz, F. Réveret, F. Médart, P. Disseix, J. Leymarie, M. Mihailovic, D. Solnyshkov, G. Malpuech, J. Zuniga-Pérez, F. Semond, M. Leroux, S. Bouchoule, X. Lafosse, M. Mexis, C. Brimont, and T. Guillet, *Phys. Rev. B* **85**, R121201 (2012).
- <sup>58</sup>B. Sermage, S. Long, I. Abram, J. Y. Marzin, J. Bloch, R. Planel, and V. Thierry-Mieg, *Phys. Rev. B* **53**, 16516 (1996).
- <sup>59</sup>T. K. Paraiso, M. Wouters, Y. Léger, F. Morier-Genoud, and B. Deveaud-Plédran, *Nat. Mater.* **9**, 655 (2010).
- <sup>60</sup>Y. G. Rubo, A. V. Kavokin, and I. A. Shelykh, *Phys. Lett. A* **358**, 227 (2007).
- <sup>61</sup>C. Ciuti, V. Savona, C. Piermarocchi, A. Quattropani, and P. Schwendimann, *Phys. Rev. B* **58**, 7926 (1998).
- <sup>62</sup>M. Wouters, *Phys. Rev. B* **76**, 045319 (2007).
- <sup>63</sup>M. Vladimirova, S. Cronenberger, D. Scalbert, K. V. Kavokin, A. Miard, A. Lemaître, J. Bloch, D. Solnyshkov, G. Malpuech, and A. V. Kavokin, *Phys. Rev. B* **82**, 075301 (2010).
- <sup>64</sup>A. I. Tartakovskii, D. N. Krizhanovskii, and V. D. Kulakovskii, *Phys. Rev. B* **62**, R13298 (2000).
- <sup>65</sup>R. Cerna, Ph.D. thesis, Thèse n° 5014, Ecole Polytechnique Fédérale de Lausanne, Switzerland, 2011; R. Cerna, T. K. Paraiso, Y. Léger, M. Wouters, F. Morier-Genoud, M. T. Portella-Oberli, and B. Deveaud-Plédran, presented at the 11th International Conference on Physics of Light-Matter Coupling in Nanostructures, Berlin (2011) (unpublished).
- <sup>66</sup>D. S. Chemla, D. A. B. Miller, P. W. Smith, A. C. Gossard, and W. Wiegmann, *IEEE J. Quantum Electron.* **20**, 265 (1984).
- <sup>67</sup>We use an expression similar to the one for the dissociation of excitons in free electron-hole pairs, see M. Colocci, M. Gurioli, and A. Vinattieri, *J. Appl. Phys.* **68**, 2809 (1990).
- <sup>68</sup>D. S. Citrin, *Phys. Rev. B* **47**, 3832 (1993).
- <sup>69</sup>P. Corfdir, A. Dussaigne, H. Teisseyre, T. Suski, I. Grzegory, P. Lefebvre, E. Giraud, J.-D. Ganière, N. Grandjean, and B. Deveaud-Plédran, *J. Appl. Phys.* **111**, 033517 (2012).